Nanoscale

PAPER

View Article Online
View Journal | View Issue

Cite this: *Nanoscale*, 2025, **17**, 7244

Inhibitory effects on smooth muscle cell adhesion and proliferation due to oscillating electric fields by nanogenerators†

Zulmari Silva Pedraza,[a] Fengdan Pan,[a] Pengfei Chen,[a] Steven Melendez Rosario,[a] Grace Wu,[a] Derui Wang,[a] Jooyong Kim,[b] Qianfan Yang,[b] Bo Liu*[b] and Xudong Wang*[a]

Received 25th October 2024,
Accepted 3rd February 2025

DOI: 10.1039/d4nr04405c

rsc.li/nanoscale

A common complication of the removal of atherosclerotic plaques or thrombi deposits to restore blood flow is restenosis. It is known that the excessive adhesion and proliferation of smooth muscle cells (SMCs) is the primary reason for restenosis. In this work, we conducted an *in vitro* study to show that a weak oscillating electric field (EF) generated by a mechanically-driven nanogenerator could prohibit SMC adhesion and proliferation on a substrate surface. Our results revealed a decrease in the cell number when an oscillating EF was introduced underneath the substrate. The cell coverage was found to be dependent on the EF strength and oscillating frequency, where higher EF strength and frequency yielded a stronger inhibitory effect. Compared to the control, this reduction in cell coverage reached up to 54% under the optimal EF parameters. This inhibitory effect was attributed to the EF-induced surface charge oscillation, which weakened the electrostatic interaction between the cell membrane and substrate. Our discovery suggests the potential for self-powered anti-restenosis solutions by integrating NG-induced oscillating EFs with biomedical device surfaces.

Introduction

Atherosclerosis is the leading cause of vascular disease worldwide.[1] It is characterized by the buildup of plaques in the inner lining of the artery wall, resulting in the thickening and hardening of arteries.[2] The atherosclerotic plaques are composed of lipids, dead cells, and inflammatory cells, all encapsulated by a fibrous cap made up of smooth muscle cells, collagen, macrophages, and other immune cells.[3] These plaques typically form in the high-pressure arterial system, especially where arteries branch, as blood flow becomes turbulent in these areas, triggering a pro-inflammatory response.[4] Plaques with thick fibrous caps are considered stable; however, when the fibrous cap becomes too thin, the plaque can rupture and subsequently lead to heart attacks and stroke. For symptomatic patients with occlusive or unstable plaques, vascular interventions such as angioplasty and stenting are employed to unblock the atherosclerotic plaque and/or thrombi deposits and restore blood flow to downstream organs and tissues.[5–7] While these vascular interventions are effective in restoring blood flow, their long-term efficacy is limited by a commonly occurring process called restenosis or the re-narrowing of arteries.[8]

The development of restenosis is primarily driven by the excessive adhesion and proliferation of smooth muscle cells (SMCs) at the site of intervention.[9] As schematically shown in Fig. 1a, this process begins with endothelial injury and inflammation.[10] During angioplasty or stent placement, the endothelial lining of the artery is often damaged, triggering an inflammatory response.[11] The combination of endothelial injury and inflammation results in the activation of SMCs, the predominant cell types residing in the medial layer.[12] Once activated, these normally quiescent SMCs migrate from the media to the intima (the innermost layer of the vessel), proliferate, and produce the extracellular matrix (ECM). The accumulation of proliferating SMCs and the ECM causes the treated arteries to thicken and narrow, leading to a reduction in the diameter of the artery and thereby a reduction in blood flow.

Several preventive and therapeutic strategies have been developed to prevent or treat restenosis.[13] Drug-eluting stents (DESs) slowly release anti-migratory and anti-proliferative drugs that inhibit SMC proliferation and migration, thereby reducing the incidence of restenosis.[14,15] Drug-coated balloons (DCBs) deliver drugs directly to the arterial wall during angioplasty, helping to suppress SMC activity that leads to

[a]*Department of Materials Science and Engineering, University of Wisconsin-Madison, Madison, Wisconsin 53706, USA. E-mail: xudong@engr.wisc.edu*
[b]*Department of Cell and Regenerative Biology, University of Wisconsin-Madison, Madison, WI 53792, USA. E-mail: bliu24@wisc.edu*

†Electronic supplementary information (ESI) available. See DOI: https://doi.org/10.1039/d4nr04405c

restenosis.[16,17] Targeting inflammation using corticosteroids or specific anti-inflammatory agents has also been shown to mitigate the early inflammatory response.[18]

Oscillating electric fields (EFs) have been shown to influence cellular behaviour, including cell adhesion, migration, and proliferation.[19,20] Recently, we discovered that a low-frequency and weak alternating EF could effectively prevent the attachment of biological species.[21] While the EF used in this study had a much lower intensity than those used conventionally, it exhibited a significant anti-attachment effect by disturbing the surface electrical double layer, which subsequently disrupts the electrostatic force between the organics and substrate. Considering that electrostatic attraction is a common mechanism for cells to form an initial attachment to surfaces, we hypothesize that a low intensity alternating EF may prevent SMCs from adhering to the endothelium, thereby inhibiting the subsequent buildup of SMCs. To test this hypothesis, we developed a device that produces a weak oscillating EF *in vitro via* a mechanically-driven nanogenerator (NG).[22–25] The optimal parameters for the oscillating electric fields, including frequency and amplitude, were investigated to achieve the desired inhibitory effects on SMCs. This study revealed a novel drug-independent anti-restenosis mechanism that could be harnessed in implantable vascular devices.

Results and discussion

Since SMC proliferation is a critical step contributing to restenosis (Fig. 1a), we designed and constructed an *in vitro* experimental setup to study the effects of EFs on SMC proliferation. As schematically shown in Fig. 1b, a pair of insulated Au interdigitated electrodes was deployed to apply the EF to the substrate surface. The electrode pair has a spacing of 100 μm with a finger thickness of 100 μm and a length of 1 cm, covering a total area of 4 × 1 cm^2 (Fig. 1c-i and Fig. S1†). This design of the electrodes ensures uniform distribution of the electric field across the cell-seeded substrate, allowing for precise modulation of cellular activity. The entire electrode and substrate surface was covered with a thin and flexible film of polydimethylsiloxane (PDMS) with inherent biocompatibility and chemical stability, preventing current leakage and providing a benign surface for cell growth. The optical transparency of PDMS contributed to clear microscopy and cell staining imaging. The two leads of the electrodes were connected to an external NG that was driven by mechanical forces to provide controlled voltage outputs. At the time of cell seeding, these PDMS coated substrates were placed in 6 cm cell culture plates and covered with culture media containing a suspended SMC line, mouse vascular smooth muscle cell (MOVAS) (Fig. 1c-ii). During the test, the external NG was pressed by a linear actuator at controlled forces and frequencies (Fig. S2†) and generated regular output voltage peaks. Fig. 1d shows a typical voltage output profile used in the study with a peak-to-peak voltage of 3.99 V at a frequency of 1 Hz. This voltage was directly applied to the interdigitated electrodes, inducing an oscillating EF at the substrate surface with specific frequencies and amplitudes.

As shown in Fig. 2a, specific areas were delineated on the electrode substrate surface to identify the influences of the NG-induced oscillating EF. The area in between the electrode fingers was labelled as "middle" (M), while the regions on the

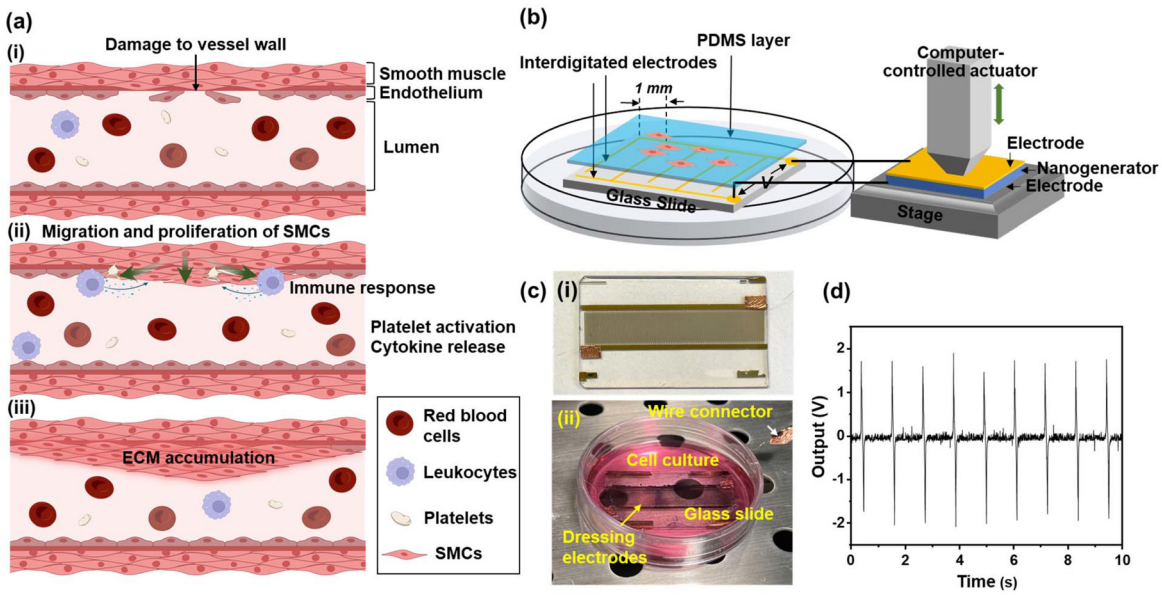

Fig. 1 Experimental setup for anti-restenosis testing. (a) Schematic of restenosis by SMCs after vessel wall injury. (b) Schematic showing the EF experimental setup. (c) Images of substrates used for MOVAS cell culture: (i) image of the prepared electrode substrates and (ii) image of the connected substrate in a cell culture dish inside an incubator. (d) Representative voltage output measurement from the external nanogenerator.

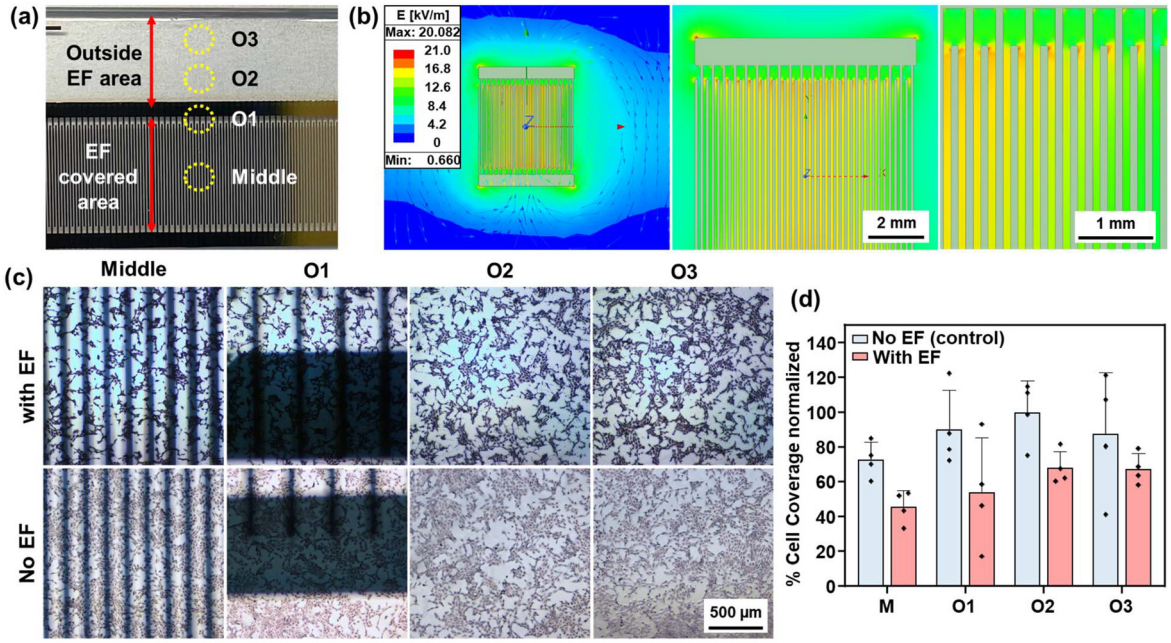

Fig. 2 Cell staining and imaging for data collection and coverage analysis. (a) Image of interdigitated electrodes detailing the location of imaging. (b) Finite element simulation showing the EF distribution on and in the vicinity of the electrode pair. (c) Images of GIEMSA stained MOVAS cells taken from different areas on the electrode substrates when the NG-induced EF was present (top) and without the EF (bottom). (d) Graph comparing the cell coverage percentages in different areas between the stained images and showing the cell coverage expressed as a percentage of the total area analysed on the slide.

substrate without electrodes buried underneath (*i.e.* outside the influence of the EF) were labelled as "outside" (O). To better understand the spatial distribution of the EF, finite element simulation was used to model the EF distribution inside and outside of the electrode covered area. As shown in Fig. 2b, the EF had a uniform distribution in the area in between the electrodes, which also had the highest strength. In the region outside the electrode zone, the EF strength decreased monotonically and reached only 10% of the strength in the middle area at a distance of 4 mm away from the electrodes. Therefore, analysing the cell coverage results could directly reflect the influence of EF strength.

This electrode substrate was connected to the actuated NG and placed in a 6 cm cell culture dish and 1.0×10^6 MOVAS cells suspended in 5 mL of culture media were added on top. The same cell culture conditions were used without connecting to the NG and therefore in the absence of EF, it served as a control. After the 24 h incubation period, the cells on the surface of the substrates were stained for imaging. As the cells on the surface were distributed nearly as a monolayer, we used the coverage by the stained cells to represent the number of cells growing on the substrate (Fig. S3†). Representative stained cell images at different locations from both experiment and control substrates are shown in Fig. 2c. In the middle area, where the EF was strongest, there was a noticeable reduction in cell coverage compared to the same area on the control substrate without the EF influence. This suggests that the EF effectively inhibited cell adhesion and proliferation in this central region. Moreover, as we moved away from the center towards the edge of the electrode covered area (O1) and further to 0.40 cm (O2) and 0.20 cm (O3) away from the electrode edge, the cell coverage increased significantly. This gradient of cell density increase exhibited a good accordance with the reduction of EF strength from the center to the outside of the electrode-covered area. Image analyses quantified the average cell coverage at each area (Fig. 2d). It clearly showed that all four selected areas in the control substrate had insignificant variations in cell coverage. The slight cell coverage gradients were likely due to cell crowding and contact inhibition from the middle area. These results suggest that in the absence of EF, the cell growth was not affected or decreased. Cells appeared uniformly distributed without EF. In general, all four selected areas in the experiment substrate had significantly lower cell coverage. Particularly, we could observe a sharp decrease from 72.69% to 45.48% when comparing the middle area of the control slides and the ones exposed to EF after 24 h of incubation. Along the edge of electrodes (O1), a decrease of 32.61% was observed between the control and experiment substrates, which was similar to the O2 area (32.05% decrease). The cell coverage difference was reduced to 36.52% on the edge (O3), where the EF strength was the weakest. The increase of cell coverage indicates a diminishing influence of the EF moving away from the electrodes. These observations corroborated our hypothesis that localized oscillating EFs can modulate cell attachment and prevent excessive smooth muscle cell proliferation.

pH examination of both control and EF groups showed that the pH values of the culture media were not influenced by the

application of EF (Fig. S4†), and therefore cell proliferation was not caused by pH change. We further investigated the influence of the applied voltage amplitude on MOVAS surface coverage. The applied voltage was adjusted by switching the load resistor in the circuit, where a higher resistance yielded a higher voltage applied to the cell culture. Fig. 3a shows the measured voltage profile with the peak-to-peak voltages of 1.73 V, 3.19 V and 3.99 V while maintaining a constant frequency of 1 Hz. Stained images revealed that all the substrates at different voltages showed a similar variation in cell density change following the EF strength distribution (Fig. S5–S7†). To quantify this location dependence, the cell coverage at four selected distances from the center of the electrodes was quantified by image analyses (Fig. 3b). Similarly, all the substrates with applied EF had a lower cell coverage compared to the control substrates. A clear increasing trend in cell coverage could be observed as the location moved from the middle to the outer regions of the substrate, where the influence of the EF was weaker. This gradient in cell distribution highlights the spatial specificity of the electric field's inhibitory effects on MOVAS proliferation under all different voltages. This location-dependent effect further supports the hypothesis that the EF has a localized impact on cell adhesion that is dependent on its strength.

Considering the middle area has the most representative cell inhibitory effect under EF influences, the cell coverage in this area under different voltages was collected and compared together with the control (Fig. 3c). By normalizing the coverage on the control substrate to 100%, it could be clearly observed that higher voltages resulted in more significant reductions in cell coverage. Under 1 V, the relative cell coverage decreased to 78.58%. As the voltage increased to 3 V and 4 V, the relevant cell coverage further reduced to 65.50% and 62.56%, respectively. There seemed to be a saturation effect at a relatively high voltage of 3 V and 4 V, as the relevant cell coverage further reduced to 65.50% and 62.56%, respectively. There seemed to be a saturation effect at a relatively high voltage of 3 V and 4 V, indicating that further increasing the voltage may not introduce a greater influence in further decreasing the cell coverage.

The relationship between oscillating frequency and cell coverage was further explored using the same experimental setup. Fig. 4a shows the voltage output profiles that were used in the frequency-relationship test, where 0.5 Hz, 1 Hz and ~7 Hz were applied to cover the normal frequency range that could be accessed by the human body. To maximize the EF effect, the voltage outputs were set at the saturation value near 4 V. It should be noted that the NG output intensity was directly related to the driving frequency. Therefore, a much higher voltage amplitude of ~21.60 V was obtained at the highest frequency of 7 Hz. As these amplitudes were beyond the saturation voltage, we assume the amplitude contribution would be minimal. The image analysis of the cell coverage on different electrode-covered/uncovered areas for the control and experimental groups is illustrated in Fig. 4b and c, respectively. The quantified graphs in Fig. 4c demonstrate a pronounced trend where escalating the frequency of the applied EF corresponds to a substantial diminution in cell coverage on the substrate surface. At the lower frequencies of 0.5 Hz and 1 Hz, the relative cell coverage was observed to decline to 39.61% and 40.66%, respectively. This reduction became more pronounced as the frequency was increased to 7 Hz, where cell coverage further diminished to 28.76%. This inverse correlation between frequency and cell coverage suggests that higher fre-

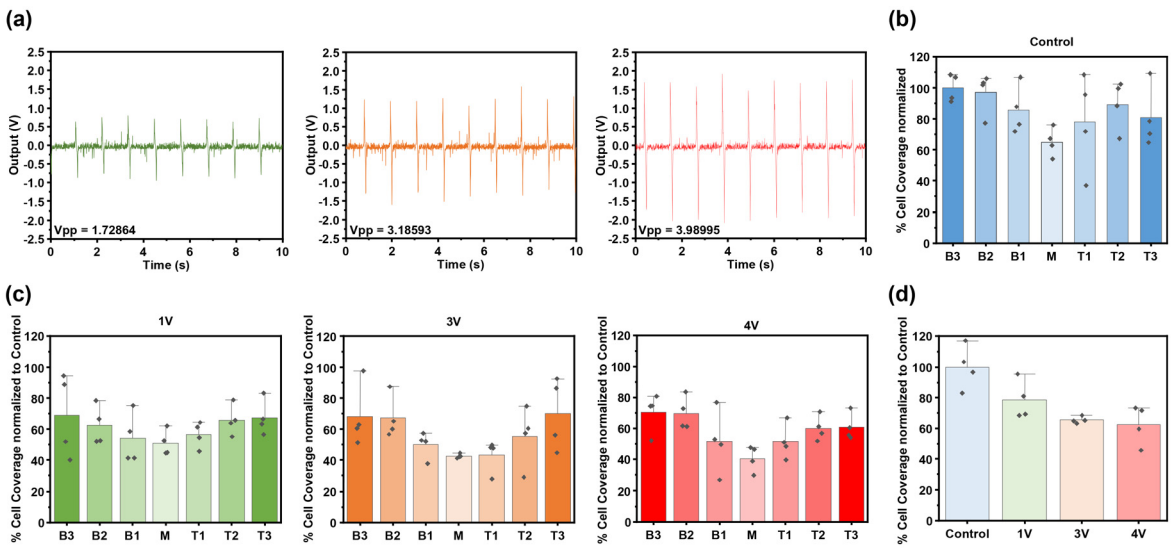

Fig. 3 Cell coverage and applied voltage relationship. (a) Voltage output measured from the NG with 1 V, 3 V and 4 V for experimental cell culture conditions. (b) Corresponding cell coverage analysis of MOVAS cultured on electrodes with no applied voltage (control). (c) Cell coverage analysis of MOVAS cultured on electrodes with 1 V, 3 V and 4 V of applied voltage to test the EF influences. (d) Comparison of cell area coverage (normalized by the control) in the middle area under different applied voltages.

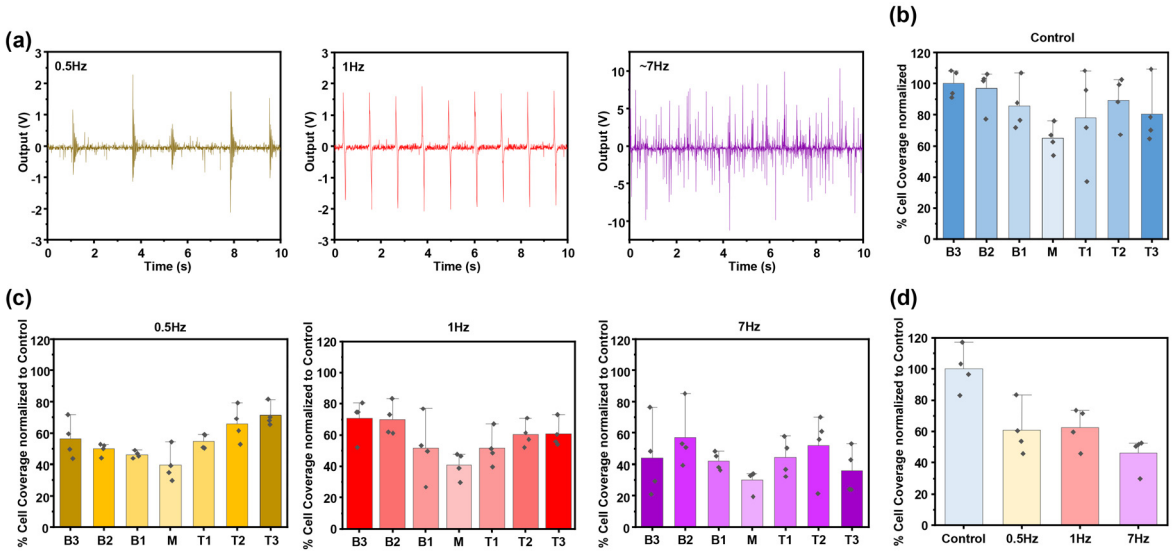

Fig. 4 Cell coverage and frequency relationship. (a) Voltage output measured from the NG at 0.5 Hz, 1 Hz and 7 Hz for experimental cell culture conditions. (b) Corresponding cell coverage analysis of MOVAS cultured on electrodes with no applied voltage (control). (c) Cell coverage analysis of MOVAS cultured under 0.5 Hz, 1 Hz and 7 Hz stimulations to test the frequency influences. (d) Comparison of cell area coverage (normalized by the control) in the middle area under different applied frequencies.

quencies of EF would exert a more potent inhibitory effect on cell adhesion and proliferation. From the direct comparison of the middle area between all conditions (Fig. 4d), the frequency-dependent inhibitory effect could be clearly observed. As the frequency increased from 0.5 Hz to 1 Hz, the average cell coverage difference was minimal (1.76%), which fell within the range of error, indicating that a small change of frequency of 0.5 Hz might not introduce significant EF influences. In contrast, when the frequency was increased to 7 Hz, an appreciable decrease to 46.12% cell coverage was observed compared to the control groups. This is a 14.68% and 16.44% decrease from the 0.5 Hz and 1 Hz conditions, respectively. This result suggests that higher frequencies disrupt the cell's ability to adhere and proliferate on the substrate more effectively than lower frequencies.

Based on the fundamentals of the cell adhesion principle, we suggest that the anti-adhesion effect could be attributed to the surface charge disturbance due to the presence of an oscillating EF. It is known that MOVAS cell membranes are charged negatively. When adhering to a substrate surface, they prefer positive surface charge to form initial bonding through electrostatic interaction. As schematically illustrated in Fig. 5a, when a voltage is applied to the two electrodes by a NG, an EF is induced at the area in between. This EF drives the redistribution of surface charge in the electrical double layer, *i.e.* positive and negative ions move toward the negative and positive electrodes, respectively. This surface charge redistribution can lead to opposite surface-cell membrane interactions. In the positive charge accumulation area, the negatively charged cell membrane experiences enhanced attraction force to the substrate, while in the negative charge accumulation area, the cell membrane experiences a repulsive force instead. As the charges reverse due to EF oscillation, the electrostatic force experienced by the cell membrane reverses accordingly. This constant switching of attractive and repulsive forces prevents a stable interaction of the cell membrane with the substrate. Therefore, it inhibits stable adhesion and proliferation of the MOVAS on the EF-covered surfaces.

It should also be noted that similar EF signals have been used for promoting cell migration and proliferation, for example, for wound healing applications.[26] This effect may seem counterintuitive to our discovery in this work. We highlight that the key difference lies in the specific parameters and configuration of the EF. Our inhibitory phenomenon relies on the EF in between a pair of electrodes that are insulated from the cell environment. There was no electric current flow through the cell environment. In contrast, the setup for promoting cell proliferation requires an electric current flow through the cell culture media to stimulate cell activities.[20,27–29] To further prove the difference between these two effects, we conducted a set of experiments to compare the distinguishing influences of electric potential and electric current. Using the same cell culture setup, we utilized electrodes without the PDMS insulating coating. As such, the electrodes were completely exposed to the cell culture media, where electric current could be induced through the media when an EF was introduced to the electrode. As shown in Fig. 5b, in (ii) under the electric current stimulation, the cell coverage was obviously higher than that on the (i) control surface, where there was no EF applied. Quantitative analysis revealed that the cell coverage increased by 48.95% as compared to that in the control (Fig. 5c). This result was opposite to the inhibitory results we observed from insulating electrodes, confirming the opposite contribution from current and potential stimulations.

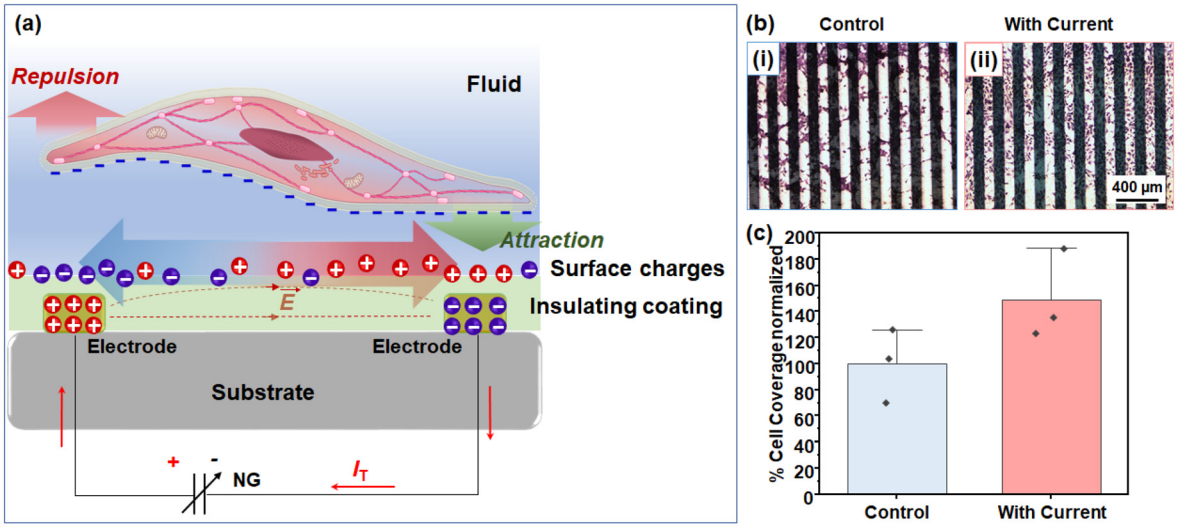

Fig. 5 Proposed mechanism underlying the inhibitory effect of oscillating EFs on cell adhesion control. (a) Schematic showing the oscillating electric field's MOVAS repelling mechanism *via* disturbance of the electric double layer in liquid media. (b) Representative images of (i) the control group, with cultured cells over exposed electrodes (no PDMS coverage) under controlled conditions and (ii) the experimental group, with cells cultured over exposed electrodes and subjected to current exposure, and (c) the corresponding cell coverage analysis.

Therefore, it was proved that cells directly exposed to electric current were promoted to spread and propagate, while cells under EF without current going through were inhibited for adhesion and proliferation. In addition, many studies have demonstrated that direct electric current stimulation promotes actin cytoskeleton reorganization and focal adhesion turnover, facilitating fibroblast migration and extracellular matrix alignments.[30–33] Some research also attributed the EF effects on cells to different membrane potentials.[33,34] These contributions are important to provide further quantitative understanding of the EF's inhibitory effects we observed on SMCs. However, our current EF setup is limited to the observations of only the cell surfaces using a stereomicroscope. A new setup that allows unblocked optical imaging, such as using transparent electrodes, would be recommended in future studies to advance the understanding and application of this intriguing effect.

Conclusion

In summary, we performed an *in vitro* study to investigate the influence of oscillating EF on the adhesion and proliferation of MOVAS cells. By applying an oscillating EF from an externally connected NG to the electrode pairs underneath the cell culture environment, we demonstrated a significant reduction in the coverage of cells at the electrode-covered area where the EF was uniformly distributed with the highest strength. The influences of both applied voltage amplitude and frequency on MOVAS surface coverage were investigated. It was discovered that higher voltages resulted in more significant reductions in cell coverage, which might saturate at ~4 V. Increasing the frequency of the applied EF was found to be correlated with the reduction in cell coverage as well. The mechanism underlying this inhibitory effect is believed to involve the interference of the EF with the electrostatic interaction between the cell membrane and substrates. An oscillating EF likely disrupts the stable surface charge distribution and thereby weakens the initial cell attachment that is necessary for cellular adhesion and proliferation. This discovery could lead to the development of self-powered devices that repel cells without the need for drugs or surgical interventions, alleviating complications associated with restenosis. More broadly, by leveraging the ability of EFs to modulate the cell–substrate interaction, these effects may also be designed to prevent unwanted bacteria or other cells from adhering, thereby enhancing the performance and longevity in diverse clinical settings.

Experimental section

Au electrode substrate preparation

To make working electrodes, 50 nm of Au was evaporated over a 5 nm Ti sticky layer onto glass slides using stainless steel masks that resulted in 100 μm wide interdigitated electrodes spaced 100 μm apart. Au wire contacts were attached to each side of the connected fingers using copper tape. These electrodes were then covered with an ~450 μm-thick layer of PDMS. The PDMS surface was treated with oxygen plasma using a PE-200 oxygen plasma surface treatment and etching system (O_2 flow rate of 8 cc min^{-1}, t = 20 s, RF = 100 W) to make the surface hydrophilic for better cell adhesion.

Cell culture setup

1.0×10^6 murine vascular smooth muscle cells purchased from the American Type Culture Collection (ATCC, CRL-2797) were

cultured in 6 cm dishes (Corning 430166). Four dishes had the UV-sterilized experimental electrode substrates, where the EF was applied from an externally connected NG. The triboelectric NG device comprised three layers of materials, namely two electrodes (80 μm, 40 × 40 mm) and a fluorinated ethylene propylene (FEP) film (50 μm). The copper electrode (on the stationary side) acted as the positive triboelectric material and also served as the induction electrode. The FEP film was attached to the other copper electrode (on the moving side) as a negative triboelectric material. The FEP film could generate a negative charge on the surface after contact with top copper electrodes due to different electron adsorption capacities. When the device was continuously driven by a motor, the two layers of the material went through a process of continuous contact and separation, through which the device produced electrical pulses to the cell culture system. The moving side of the NG was secured on the actuator's arm that was placed 3 cm away from a 3D printed base that held the stationary contact of the NG. The computer-controlled actuator cyclically moved the NG at a speed of 30, 60 or 420 rpm to control the frequency. The NG output was measured using a multimeter (DMM 6500, Keithley, internal resistance 10 MΩ) connected to the substrate electrodes. The output voltage was controlled by connecting a resistor in parallel with the electrode pair, where a larger resistance yielded a higher voltage amplitude on the electrodes. Resistors of resistances 330 kΩ, 680 kΩ and 1.5 MΩ were used, which achieved outputs of 1 V, 3 V and 4 V respectively. Four dishes containing PDMS-coated electrode substrates but without the EF were used as controls. All the dishes were cultured in modified DMEM containing 4.5 g L^{-1} D-glucose (Thermo Scientific, 11965118) supplemented with 10% fetal bovine serum (FBS), 100 U mL^{-1} penicillin, and 100 U mL^{-1} streptomycin and incubated for a total of 24 h. After treatment, all plates were stained with GIEMSA stain to observe the internal structure of the cells for ease of localization and quantification.

Cell staining protocol

The plates were removed from the incubator, the culture media were removed and the surface of the substrates was washed with PBS. The cells were then fixed with 4% paraformaldehyde for 15 min at room temperature and rinsed again with PBS. Afterwards, 5 ml of GIEMSA stain (Sigma-Aldrich GS500-500 ml) was applied over each slide for 10 minutes. The slides were then washed with PBS and dried in an oven at 55 °C. The stained slides were stored at 4 °C until the time of imaging.

Optical microscopy imaging

All slides were categorized into three sections and imaged using a Nikon ECLIPSE Ti optical microscope. One section showcases three images covering the top area, another section displays three images occupying the bottom area, and the final section features an image covering the middle area with the electrodes. Each of these images was captured using a microscope at a resolution of 1280 × 1024 pixels.

pH measurements

Each dish was filled with 5 mL of high-glucose Dulbecco's modified Eagle's medium (DMEM, Thermo Fisher) without cells. In the EF group, the electrodes were connected to an electric circuit to generate an electric field, while the control group was left unconnected. All dishes were incubated at 37 °C with 5% CO_2 for 24 hours. pH measurements were taken at baseline and after 24 hours of incubation. Baseline pH was measured using a 5 mL aliquot of high-glucose DMEM collected at the start of the experiment. After 24 hours, 5 mL samples were collected from each dish for pH measurement. All measurements were performed using a pH per mV meter (FiveEasy Plus FP20, Mettler Toledo) in accordance with the manufacturer's instructions. The results were analyzed using a two-way analysis of variance (ANOVA) model with multiple comparisons performed in PRISM software (GraphPad Software).

Image processing and analysis

The pixels in the captured images were utilized as coordinates to accurately locate the section under analysis (Fig. S8†). Frames were chosen according to their position on the x and y axes, as well as their width and height dimensions. The frames used were 600 × 420 for areas without electrodes, while 200 × 600 and 125 × 960 were designated for rectangles that avoided electrode shadows. ImageJ macro was used after identifying the desired frame to execute the following series of commands: crop the image, convert it into 16-bit RGB [image > type > RGB stack, 16-bit], and launch the threshold adjustment to be manually manipulated until obtaining the most accurate percentage of cell area coverage. The threshold adjustment consists of two intensity values that convert everything below into white and everything above into black, allowing a red surface over the desired area. Once the surface covering the MOVAS cells is selected, the area coverage is measured obtaining the mean and the % area value.

NG output measurement

To measure the output voltage from the NG, both sides of the NG electrodes were taped with Cu foils as electrodes. Under continuous compressive force, the output was collected by a multimeter (DMM 6500, Keithley, internal resistance 10 MΩ) and then plotted using Origin software.

Scanning electron microscopy imaging

The size and dimensions of the evaporated electrodes were confirmed through SEM imaging using a Zeiss LEO 1550VP SEM at a 3.00 kV accelerating voltage and a working distance of 8 mm.

Data availability

The data supporting the findings of this study are available within the article and its ESI,† as well as from the corresponding author upon reasonable request.

Conflicts of interest

There are no conflicts to declare.

Acknowledgements

This work was supported by the National Institutes of Health under award number R01HL157077 and the University of Wisconsin-Madison Office of the Vice Chancellor for Research and Graduate Education with funding from the Wisconsin Alumni Research Foundation. ZSP thanks the Graduate Engineering Research Scholars (GERS) for funding by the Advanced Opportunity Fellowship (AOF), through the support of the State of Wisconsin and the University of Wisconsin Graduate School.

References

1 W. Herrington, B. Lacey, P. Sherliker, J. Armitage and S. Lewington, *Circ. Res.*, 2016, **118**, 535–546.
2 J. F. Bentzon, F. Otsuka, R. Virmani and E. Falk, *Circ. Res.*, 2014, **114**, 1852–1866.
3 J. L. M. Björkegren and A. J. Lusis, *Cell*, 2022, **185**, 1630–1645.
4 P. Libby, *Arterioscler., Thromb., Vasc. Biol.*, 2012, **32**, 2045–2051.
5 J. S. Lawton, J. E. Tamis-Holland, S. Bangalore, E. R. Bates, T. M. Beckie, J. M. Bischoff, J. A. Bittl, M. G. Cohen, J. M. DiMaio, C. W. Don, S. E. Fremes, M. F. Gaudino, Z. D. Goldberger, M. C. Grant, J. B. Jaswal, P. A. Kurlansky, R. Mehran, T. S. Metkus, L. C. Nnacheta, S. V. Rao, F. W. Sellke, G. Sharma, C. M. Yong and B. A. Zwischenberger, *Circulation*, 2022, **145**, e4–e17.
6 E. Violari, A. Payomo, B. J. Schiro, A. Powell, R. T. Gandhi and C. S. Pena, *Tech. Vasc. Interv. Radiol.*, 2022, **25**, 100840.
7 J. A. Beckman, P. A. Schneider and M. S. Conte, *Circ. Res.*, 2021, **128**, 1885–1912.
8 D.-M. Zhang and S. Chen, *Cardiol. Res. Pract.*, 2020, **2020**, 8104939.
9 S. Déglise, C. Bechelli and F. Allagnat, *Front. Physiol.*, 2023, **13**, 1081881.
10 R. Kenagy, in *Mechanisms of Vascular Disease: A Reference Book for Vascular Specialists*, ed. R. Fitridge and M. Thompson, The University of Adelaide Press, 2011, pp. 115–152, DOI: 10.1017/UPO9781922064004.008.
11 D. Kotschy, M. Kotschy, L. Masłowski, P. Socha, J. Kwapisz, A. Czyżewska-Buczyńska, M. Karczewski and W. Witkiewicz, *Acta Angiol.*, 2014, **20**, 47–59.
12 S. O. Marx, H. Totary-Jain and A. R. Marks, *Circ.: Cardiovasc. Interventions*, 2011, **4**, 104–111.
13 Y. Gouëffic, G. Torsello, T. Zeller, G. Esposito, F. Vermassen, K. A. Hausegger, G. Tepe, M. Thieme, M. Gschwandtner, A. Kahlberg, M. Schindewolf, M. Sapoval, J. Diaz-Cartelle, K. Stavroulakis, L. Apruzzi, D. Baccellieri, F. Bea, J.-P. Becquemin, C. Bent, L. Bertoglio, A. Bianchini, T. Bieri, E. Blessing, P. Chaillou, R. Chiesa, C. Del Giudice, K. Deloose, P. Desgranges, C. Erbel, C. Espinola-Klein, G. Esposito, P. Feugier, I. Fourneau, G. Grözinger, M. Gschwandtner, L. Guillemot, M. Hamady, K. A. Hausegger, B. Heilmeier, J. Hendriks, O. Jaffer, A. Kahlberg, N. Kakani, K. Keirse, C. Kranewitter, M. Krokidis, R. Langhoff, M. Lee, P. Lohle, L. Maene, A. Mahnken, L. Maiwald, D. Mascia, A. Melloni, P. Montorsi, C. Nice, A. Oberhuber, C. Paetzel, G. Ramjas, C. Rammos, E. Rinaldi, E. Rosset, R. Ruiz Salmeron, M. Sapoval, C. Saracino, A. Sauguet, J. P. Schäfer, N. Schahab, M. Schindewolf, N. Settembre, E. Simonini, J. Sobocinski, E. Steinmetz, G. Tepe, F. Thaveau, M. Thieme, G. Torsello, H. van Overhagen, F. Vermassen, J. Verbist, T. Zeller and N. Zorger, *Circulation*, 2022, **146**, 1564–1576.
14 M. M. P. C. Donners, M. J. A. P. Daemen, K. B. J. M. Cleutjens and S. Heeneman, *Ann. Med.*, 2003, **35**, 523–531.
15 M. A. Costa and D. I. Simon, *Circulation*, 2005, **111**, 2257–2273.
16 N. Montelione, V. Catanese, A. Nenna, M. Jawabra, E. Verghi, F. Loreni, F. Nappi, M. Lusini, C. Mastroianni, F. Jiritano, G. F. Serraino, P. Mastroroberto, F. A. Codispoti, M. Chello, F. Spinelli and F. Stilo, *Diagnostics*, 2022, **12**, 2207.
17 K. Changal, M. Patel, P. P. Devarasetty, R. Royfman, S. Veria, R. Vyas, M. Mhanna, N. Patel, A. Beran, M. Burket and R. Gupta, *J. Soc. Cardiovasc. Angiogr. Interventions*, 2022, **1**, 100024.
18 S.-Y. Lee, I.-H. Bae, D. Sung Park, E.-J. Jang, J.-W. Shim, K.-S. Lim, J.-K. Park, D. S. Sim and M. H. Jeong, *J. Biomater. Appl.*, 2016, **31**, 36–44.
19 T. Taghian, D. A. Narmoneva and A. B. Kogan, *J. R. Soc., Interface*, 2015, **12**, 20150153.
20 A. Liu, Y. Long, J. Li, L. Gu, A. Karim, X. Wang and A. L. F. Gibson, *J. Nanobiotechnol.*, 2021, **19**, 280.
21 Y. Long, Y. Yu, X. Yin, J. Li, C. Carlos, X. Du, Y. Jiang and X. Wang, *Nano Energy*, 2019, **57**, 558–565.
22 M. Kang, D.-M. Lee, I. Hyun, N. Rubab, S.-H. Kim and S.-W. Kim, *Chem. Rev.*, 2023, **123**, 11559–11618.
23 X. Pu, C. Zhang and Z. L. Wang, *Natl. Sci. Rev.*, 2022, **10**, nwac170.
24 Y. Wang, Y. Yang and Z. L. Wang, *npj Flexible Electron.*, 2017, **1**, 10.
25 Y. Quan, X. Wu, S. Zhu, X. Zeng, Z. Zeng and Q. Zheng, *Med. Novel Technol. Devices*, 2022, **16**, 100195.
26 R. Luo, J. Dai, J. Zhang and Z. Li, *Adv. Healthcare Mater.*, 2021, **10**, 2100557.
27 K. Katoh, *Med. Sci.*, 2023, **11**, 11.
28 S. Mobini, L. Leppik and J. H. Barker, *BioTechniques*, 2016, **60**, 95–98.
29 Y. Long, H. Wei, J. Li, G. Yao, B. Yu, D. Ni, A. L. F. Gibson, X. Lan, Y. Jiang, W. Cai and X. Wang, *ACS Nano*, 2018, **12**, 12533–12540.

30 X.-W. Xiang, H.-T. Liu, W. Liu, Z.-Y. Yan, Y.-L. Zeng, Y.-J. Wang, J. Liu, Y.-C. Chen, S.-X. Yu, C.-H. Zhu, X.-N. Tao, C. Wang, J.-T. Wu, Y. Du, X.-X. Xu, H. Gao, Y. Jiu, J. Ma, J. Qiu and L. Chang, *Chem. Eng. J.*, 2023, **471**, 144267.
31 J. Zhang, R. Ren, X. Luo, P. Fan, X. Liu, S. Liang, L. Ma, P. Yu and H. Bai, *PLoS One*, 2014, **9**, 1–9.
32 J. Chen, Y. Liu, J. Lan, H. Liu, Q. Tang, Z. Li, X. Qiu, W. Hu, J. Xie, Y. Feng, L. Qin, X. Zhang, J. Liu and L. Chen, *CNS Neurosci. Ther.*, 2024, **30**, 1–19.
33 K. Katoh, *Life*, 2022, **12**, 531.
34 V. S. Mandala and R. MacKinnon, *Proc. Natl. Acad. Sci. U. S. A.*, 2022, **119**, 1–12.